EPJ Web of Conferences **292**, 02003 (2024) https://doi.org/10.1051/epjconf/202429202003
NRM2023

Nuclear reaction cross sections and the optical potentials and for the n-^{12}C and N-^{12}C scattering

Imane Moumene[1,3,*] and *Angela* Bonaccorso[2,**]

[1]Istituto Nazionale di Fisica Nucleare, Galileo Galilei Institute for Theoretical Physics, Largo Enrico Fermi, 2, 50125 Firenze, Italy
[2]Istituto Nazionale di Fisica Nucleare, Sezione di Pisa, Largo Bruno Pontecorvo 3, 56127 Pisa, Italy
[3]*Present Address:* Dipartimento di Fisica, Università degli Studi di Milano, Via G. Celoria 16, 20133 Milano, Italy

Abstract. In this talk we first discuss total cross sections for the system n-^{12}C in the incident energy range 20-500 MeV, calculated with a phenomenological optical potential and the optical model. We compare with calculations done with the eikonal model using the same potential and a single folding potential in the optical limit. Several single folding potentials are obtained using ^{12}C densities from different models. These potentials are sensitive to the density used and none of them reproduces the characteristics of the phenomenological potential nor the cross section results. We then discuss nucleus-nucleus potentials and reaction cross sections for some projectiles on ^{12}C within the eikonal formalism. We find that single folded projectile-target imaginary potentials and double folded potentials can produce similar energy dependence of the reaction cross sections but the single folding results agree better with experimental data provided the radius parameter of the phenomenological n-target potential is allowed to be energy dependent. We conclude that a single folding nucleus-nucleus potential build on a phenomenological nucleon-nucleus potential can constitute an interesting and useful alternative to double folding potentials.

1 Introduction

Realistic nuclear reaction cross-section models are an essential ingredient of reliable heavy-ion transport codes [1]. The therapeutic use of heavy ions, such as carbon, has gained significant interest due to advantageous physical and radiobiologic properties compared to photon based therapy [2]. Also in reactor physics data and models of reaction cross sections are of fundamental importance [3].

Two of the most used targets for measurements of total reaction cross sections and nuclear breakup with 'normal' and radioactive ion beams (RIBs), are ^{9}Be and ^{12}C. Most recently exotic nuclei close to ^{12}C, such as ^{12}N, ^{11}C and ^{10}C have been proposed for radiation therapy [4]. From the point of view of theoretical calculations, while the optical model (OM) and coupled-channel (CC) model are certainly the most accurate ways to obtain numerical reaction cross sections, the Glauber model [5] with folded potentials (f.p.) [6, 7], has also been used for many years [8, 9] and its results compared to data. Since the beginning of physics with RIBs the method has become very popular for its simplicity in deducing density distributions of exotic nuclei and their root mean square radii (r.m.s.) [10–18] and the core-target survival probability in knockout reactions [19]. Indeed from the time of the introduction of f.p.

*e-mail: imane93.moumene@gmail.com
**e-mail: bonac@df.unipi.it

Satchler [7] suggested that caution should be taken with the model, in particular when applied to obtain the imaginary part of the optical potential. A known drawback of imaginary folded potentials is that they are often too absorptive in the internal part while being too shallow on the surface. This can be a problem for exotic nuclei which are often very diffuse due to the anomalous N/Z ratios and present phenomena such as neutron halo and neutron skin. In studying the energy dependence of reaction cross sections several groups have tried to modify some of the ingredients of the double folded potential in the attempt to improve the performances of the model. For example in Ref. [12] the average neutron-proton (np) and proton-proton (pp) cross sections were modified, while in Ref. [18] the range parameter β of the effective (nn) and (np) interaction were fitted. A very detailed study of the dependence of reaction cross section calculations on the parameters of the folded potential was done in the seminal paper Ref. [21] while Ref. [22] dealt with Pauli blocking and medium effects in nucleon knockout. In general double folded potentials need to be corrected to take into account medium effects beyond the simple nn interaction.

More fundamental, microscopic approaches have been followed by several authors, see Ref. [23] for a recent, exhaustive review. For nucleon-nucleus (nN) potentials ab-initio methods have reached a quite high degree of accuracy [24–27]. On the other hand nN potentials [29] and nucleus-nucleus (NN) potentials Ref. [30–33] and other works by the same authors are based on a microscopic, complex g-matrix and then either a single folded or a double folded model is constructed. In the following we will discuss further these approaches and their results in comparison with ours.

In order to improve the calculations of NN folded potentials Satchler and Love [6] proposed single folded potentials obtained by folding a phenomenological nucleon-nucleus interaction with the density of the other colliding nucleus. The authors of Ref. [35] applied this idea by using the Bruyères Jeukenne-Lejeune-Mahaux (JLMB) model [36, 37] for the potentials folded with various projectile densities. The method from Ref. [16] called MOL, for modified optical limit can also be interpreted as a special kind of the single folded procedure that we will discuss in Eq. (4). In Ref. [16] an effective nN profile function was introduced which acts as the nN optical potential does in the single folded model. On the other hand, in Ref. [38] thanks to the existence of an almost continuous series of neutron-^{9}Be data as a function of the neutron incident energy, a phenomenological and a Dispersive Optical Model (DOM) optical potentials were introduced for the system neutron-^{9}Be which were able to reproduce at the same time the total, elastic and reaction cross sections and all available elastic scattering angular distributions. Then using one of those potentials denoted as (AB) and defined in Eq. (1) a single folded (light)-nucleus-^{9}Be imaginary optical potential was derived and it was shown that it is more accurate than a double folded optical potential [39–41] in reproducing NN reaction cross section. Of course one might wonder whether such results are due to the special nature of ^{9}Be which is itself weakly bound and strongly deformed. For this reason and to draw more general conclusions we apply in this work the same (AB) potential to the description of n-^{12}C scattering and calculate by the optical model total reaction cross sections in the range 20-500 MeV finding excellent agreement with the data. At the moment we do not attempt to fit the low energy resonance region which would need an *ad-hoc* study in particular as far as the spin-orbit potential is concerned. Experiments with exotic nuclei studied at energies larger than about 60-80A. MeV are insensitive to the low energy part on the nucleon-target cross section. However there is a large bulk of data at relativistic energies larger than 200A. MeV. Also the BARB experiment at GSI deals with high energy beams [4]. For this reason we have extended the (AB) potential to fit n-^{9}Be and n- ^{12}C total cross sections above 200 MeV, finding small differences in the two cases. Folding the newly established n- ^{12}C optical potential with several projectile densities, we will then construct single folded N-^{12}C potentials. These potentials are necessary to calculate reaction cross section and deduce from data unknown nuclear densities and r.m.s. radii, as mentioned above. They could easily be imported in transport codes. Furthermore, they are also necessary in breakup models to calculate the S-matrices for the core-target and nucleon-target scattering. In the future we plan to apply the single folded and double folded potentials to a series of exotic nuclei knockout induced reactions in order to assess their accuracy in reproducing single nucleon breakup absolute cross sections as suggested in [20]. Of course reactions with ^{12}C have been intensively studied in the past, using it both as a projectile and as a target. Due to length limitation of this paper we do not revise the large bulk of data and literature but concentrate only on the implications accurate, new potentials might have in basic studies of reaction cross sections involving exotic and normal projectiles.

Cross sections are calculated with a standard optical model and with the eikonal method using the phenomenological potential and some n-target single folded potentials. Results for the energy dependence of the total cross sections are compared.

To lend further support to our approach, similarly to what has been done in Refs. [39, 40], we will calculate the imaginary part of ^{12}C-^{12}C optical potential with the single folded and double folded methods and discuss their differences. Finally some NN reaction cross section calculations will be compared to experimental values for the systems ^{12}C+^{12}C, ^{9}Be+^{12}C. Given the symmetry of projectile and target the former system is a particularly interesting test case for the accuracy of the phenomenological potential approach vs. folded potential.

2 Theoretical model

The potential considered in this paper has the form

$$U_{AB}(r,E) = -\left[V_{WS}(r,E) + iW_{WS}(r,E)\right]. \tag{1}$$

The real part of the neutron-target interaction is given by V_{WS}, the usual Woods-Saxon potential

$$V_{WS}(r) = V^R f(r,R^R,a^R) \tag{2}$$

Also, the imaginary part takes the form

$$W_{WS}(r) = W^{vol} f(r,R^I,a^I) - 4a^I W^{sur}\frac{d}{dr} f(r,R^I,a^I). \tag{3}$$

with $f(r,R^i,a^i) = \left(1+e^{\frac{r-R^i}{a^i}}\right)^{-1}$ and $R^i = r^i A^{1/3}$.

The real (AB) potential of Ref. [38] contained also a correction term δV which originates from surface-deformation effects and represents channels for which a simple Woods-Saxon form is not appropriate. Because such couplings are important only up to around 20 MeV and here we are not interested in this low energy region for the present applications on ^{12}C we shall take δV=0. For the same reason the spin-orbit term will be neglected. The parameters of $U_{AB}(r,E)$ for the n-^{12}C interaction used in this paper are given in Table I.

Table 1. Energy-dependent optical-model parameters of the potential n-^{12}C for $E \geq$160 MeV, where E=E$_{lab}$. At lower energies, the parametrization is the same as for ^{9}Be from Ref. [38]. a^R=0.288fm at all energies.

E	V^R	r^R	W^{sur}	W^{vol}
(MeV)	(MeV)	(fm)	(MeV)	(MeV)
$160 \leq E < 200$	$31.304 - 0.145E$	$1.647 - 0.005(E-5)$	$12.7 - 0.025(E-160)$	$4.8 - 0.025(E-160)$
$200 \leq E < 215$	"	"	11.7	3.8
$215 \leq E < 220$	0	"	"	"
$220 \leq E \leq 500$	"	0.1	$11.7 + 0.02(E-220)$	$3.8 + 0.02(E-220)$

Table 2. Energy-dependent optical-model parameter r^I for the potential for n+^{12}C used in calculations of single folded NN potentials.

E (MeV)	$30 \leq E \leq 160$	$E > 160$
r^I(fm)	$1.32 - 0.0013E$	1.118

We consider also a single folded [7, 35] n-target potential U_ρ^{nT} defined as:

$$U_\rho^{nT}(\mathbf{r}) = -\frac{1}{2}\hbar v \sigma_{nn}(1 - i\alpha_{nn})\rho_T(\mathbf{r}) \tag{4}$$

Where $\rho_T(\mathbf{r})$ is the target density function for which we will use a number of different models as specified in the following, σ_{nn} is the average of the experimental neutron-proton and proton-proton cross sections and α_{nn} is the ratio of the real and imaginary scattering amplitude at zero degrees. v is the classical relative motion velocity of the scattering. The previous equation can be generalized in a obvious way in order to distinguish between the proton and neutron densities and the proton-neutron and proton-proton cross sections, using: $\rho_P = {\rho^n}_P + {\rho^p}_P$, and $U_\rho^{nT}(r) = -\frac{1}{2}\hbar v[\sigma_{np}(1 - i\alpha_{np}){\rho^p}_T(r) + \sigma_{pp}(1 - i\alpha_{pp}){\rho^n}_T(r)]$. This is the formalism followed in the present work. Here we are assuming a zero-range nucleon-nucleon interactions and the values of σ_{nn} and α_{nn} will be taken from the parametrization of Refs. [11, 14, 22].

In the case of NN scattering we will discuss potentials U^{NN}, negative defined as

$$U^{NN}(\mathbf{r}) = \int d\mathbf{b_1} U^{nN}(\mathbf{b_1} - \mathbf{b}, z) \int dz_1\, \rho(\mathbf{b_1}, z_1). \tag{5}$$

This quantity is the single folded optical potential given in terms of a nN optical potential $U^{nN}(\mathbf{r})$ and the matter density $\rho(\mathbf{b_1}, z_1)$ of the other nucleus. In the single-folding method, $U^{nN}(\mathbf{r})$ can be a phenomenological nucleon-target potential, Eq. (1), such as the (DOM) or the (AB) potentials of Ref. [38]. In the double folded method, U^{NN} is obtained from the microscopic densities $\rho_{P,T}(\mathbf{r})$ for the projectile and target respectively and an energy-dependent nucleon-nucleon (nn) cross section σ_{nn}, by using Eq. (4) for U^{nN} with the notation T=N in Eq. (5). For simplicity, we refer the readers to Ref. [39, 40] for a review of the eikonal formalism [5] including the well known formulae for the reaction cross section, phase shift, and S-matrix.

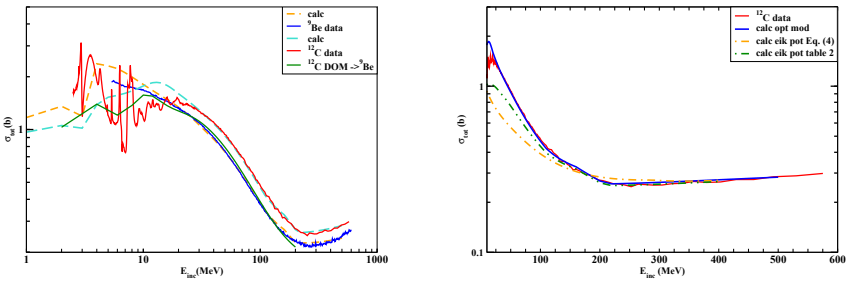

Figure 1. (Color on line) [LHS] Total experimental and calculated cross sections. Lower blue curve for n+^{9}Be, upper red curve for n+ ^{12}C. The optical model calculations are given by the orange and cyan dashed lines, respectively. The solid green line is a calculation made with a (DOM) potential obtained for n+^{12}C and applied to n+^{9}Be [43]. [RHS] Total experimental and calculated cross sections for n+ ^{12}C. Red curve for the data. Blue full curve and green double-dotted-dashed line are results of optical model and eikonal calculations respectively, with the potential Eq. (1-3) and Table 1. The orange dot-dashed line is the eikonal calculation with the single folded potential Eq. (4).

3 Results

We start by showing in Fig. 1 [LHS] the energy dependence of the reaction cross section calculated with an optical model code using the potential defined by Eq. (1-3) and the parameters given in Table 1 for

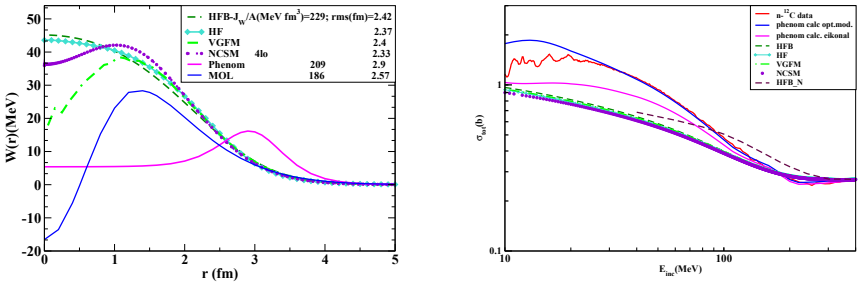

Figure 2. (Color online) [LHS] n+^{12}C potentials calculated with various model densities at 300 MeV, see legend and text. The blue line is the potential deduced from the profile function of Ref. [16]. The magenta thick curve is the phenomenological potential of Eq. (1-3) and Table 1. [RHS] Total experimental and calculated cross sections for n+ ^{12}C. The red curve represents the experimental values [42]. Blue curve is the calculation by the optical model with the phenomenological potential. The other curves are calculations using the single folded. potential Eq. (4) and Fig. 2 [LHS] using fixed α_{nn} values in Eq. (4) appropriate for 300 MeV. The brown dashed curve labelled as HFB_N uses the energy dependent α_{nn} from Ref. [11, 14, 22]. Note that they are known only from 40 MeV. See text for details.

Table 3. Comparison of the reaction cross sections of the ^{12}C+^{12}C system. Incident energies are indicated in the first column. Strong absorption radius parameter within the single and double folding methods are listed in the third column. The fourth column provides the volume integrals for active particle. The next columns contain the theoretical cross sections calculated with various densities. Before each of them are the r.m.s. radii of the corresponding imaginary potentials, some of which are shown in Fig. 3.

E_{inc}	model	r_s	J_W/A_PA_T	r.m.s	σ_{NCSM}	r.m.s	σ_{HF}	r.m.s	σ_{HFB}
(MeV)		(fm)	(MeVfm^3)	(fm)	(mb)	(mb)	(mb)		
83	single folded	1.2	184	3.72	994	3.75	1008	3.78	1025
	double folded	1.22	279	3.29	957	3.36	995	3.43	1027
300	single folded	1.18	151	3.57	760	3.60	768	3.64	780
	double folded	1.11	241	3.29	791	3.36	815	3.43	842

n+^{12}C and in Ref. [38] for n+^{9}Be. We show also the experimental data from Ref. [42]. It is interesting that the experimental data show a clear scaling between the two nuclei, accurately reproduced by the calculations. Note that the two corresponding potentials have the same radius parameter but different radii, due to the difference in mass. Otherwise the other parameters differ only above 160 MeV. Ref. [38] presented also results for n+^{9}Be from a dispersive optical potential (DOM) calculation. (DOM) potentials exist also for n+^{12}C. Indeed in the same figure the green solid line shows the results obtained for a ^{9}Be target using the (DOM) obtained for ^{12}C [43]. It is amazing that also for the (DOM) potential model, the same parametrization can be successfully applied to the two different targets. As it was found in Ref. [38] for ^{9}Be, the agreement shown here for the ^{12}C target, between data and OM calculations is remarkable and is comparable to that obtained for example in Ref. [3] where a coupled-channel (CC) technique was used. Note that also the authors of Ref. [3] stressed a similarity between parametrizations

for ^{9}Be and ^{12}C. As we shall see in the following, the advantage of a simple OP approach, with respect to CC calculations, is that it can easily be used to build folding potentials for nucleus-nucleus scattering and also it can be used in eikonal and fully quantum-mechanical models [19, 44] of knockout from exotic nuclei.

In Fig. 1 [RHS] the total experimental cross section for n+ ^{12}C is shown again by the red curve while the blue full curve and green double-dotted-dashed line are results of the optical model and eikonal calculations respectively, with the potential Eq. (1-3) and Table 1. The orange dot-dashed line is the eikonal calculation with the single folded potential Eq. (4). These results indicate that while the simple eikonal approximation with the phenomenological potential works well from about 100 MeV incident energy, the eikonal model with the folded potential starts to work well only from about 200 MeV. Clearly the Glauber and folding models miss some effects of excitation modes in the target, beyond the simple nn free scattering concept. The optical model with the phenomenological n-T potential includes instead such effects. In this respect, we first note that the U_{ρ}^{nT} potential of Eq. (4) has the same range and profile as the target density because σ_{nn} and α_{nn} are simple scaling factors. To understand better this point Fig. 2 [LHS] shows the imaginary potentials calculated at 300 MeV with the densities indicated in the legend from references [45]-[46]. Harthree-Fock-Bogoliubov (HFB) densities were calculated with the code HFBTHO [47] and the Skyrme interaction SkM* [48]. Using other Skyrme interactions does not produce substantial differences. No-Core-Shell-Model (NCSM) densities were obtained by using the nn4lo [28] interaction. We provide also the volume integrals per particle and r.m.s. values. The former (J_W/A_T) have all the same values because all densities are normalized to the number of nucleons. The latter (r.m.s.) have very similar values although in the internal parts the potentials are quite different. The phenomenological potential is completely different, being very shallow at the interior and having instead a pronounced surface peak and long tail. Its volume integral is smaller than that of the single folded potentials while its r.m.s. is quite larger. Indeed Fig. 2 [RHS] shows again the experimental cross sections as in Fig. 1 but this time besides the optical model calculation with the phenomenological potential, results of the eikonal approximation with the single folded potentials of Fig. 2 [LHS] obtained with different densities, are shown. One can notice the small effect of changing the target density. However, it is interesting to note that the cross section values seem to scale with the r.m.s. of the potential. This result suggests that only the surface behaviour of the potential (and of the target density) determines the value of the cross section, and that in turn it is only the r.m.s. radius of the target density that can be deduced from data, a confirmation of the simple geometrical nature of the Glauber model. In this figure the calculations shown as HFB_N were made from 40 MeV using the HFB density and σ_{nn} and α_{nn} taken from the parametrization of Refs. [11, 14, 22] (brown dashed curve), while in the other calculations with various densities we kept α_{nn} fixed at the value appropriate to 300 MeV just to show the small dependence on the density. Note that a precise evaluation of the α_{nn} parameters is a delicate issue which to our knowledge has not been fully resolved to date, see in particular Fig. 4 of [49].

We turn now to the study of nucleus-nucleus scattering by building a double folded potential and a single folded potential according to Eq. (5). Note that single folded refers to a potential for n-T scattering, build on the target density Eq. (4), while in the case of NN scattering single folded indicates a potential build using in Eq. (5) the projectile density and the n-T phenomenological potential Eq. (1). Double folded refers to a NN potential obtained from Eq. (4) in Eq. (5).

In Fig. 3 a number of such imaginary potentials are shown for the ^{12}C-^{12}C system at 83 and 300 MeV as indicated in the legend. We show double folded potentials obtained with the HF and No-Core-Shell-Model (NCSM) densities obtained from the nn4lo [28] interaction and single folded potentials obtained with the potential of Table 2 varying the r^I values and the NCSM and HFB densities. We will see in the following that, in order to reproduce the experimental cross sections, the r^I parameter needs to be energy dependent when the n-T phenomenological potential is used to build up the NN potential. The double folded potentials shown in the upper panel of Fig. 3 are deeper and with smaller r.m.s. radii than the single folded potentials which are characterised instead by longer tails and larger r.m.s. values while their volume integrals are smaller than those of the double folded potentials, see also Table 3. In the same table the values of calculated reaction cross sections at 83 and 300A. MeV are given. Incident energies are indicated in the first column, strong absorption radius parameters within the single and double folded methods using the HFB densities are listed in the third column while the fourth column

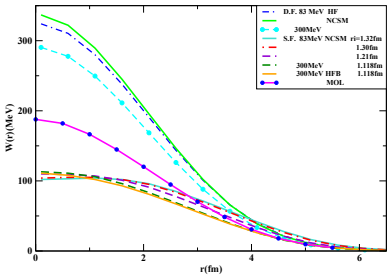

Figure 3. (Color online) Imaginary part of the ^{12}C-^{12}C optical potential at 83 and 300 MeV as indicated in the legend. The double folded potentials shown are obtained with the HF and NCSM densities. The single folded potentials are obtained with the potential of Table 2 varying the r^I values and the NCSM and HFB densities. See text for details. The full magenta line with blue dots is the MOL potential obtained from [16].

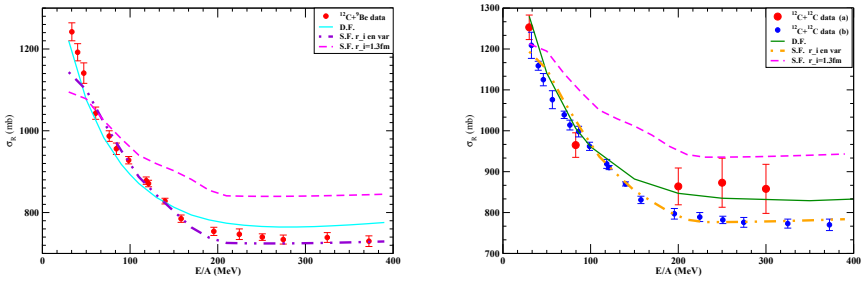

Figure 4. Comparison of experimental reaction cross sections (circles with error bars) and theoretical values within single folded and double folded potentials (dot-dashed and full lines respectively), for the scattering of ^{12}C+^{12}C [RHS] and ^{12}C+^{9}Be [LHS]. In both figures the small data points are from Ref. [12]. In the [RHS] panel the large red points (a) are from Ref. [9]. The magenta dashed lines in both panels represent the single folded results obtained using a fixed value r^I=1.3 fm for the radius parameter of the imaginary phenomenological optical potential. The dot-dashed lines correspond to an energy dependent r^I. See text for details.

provides the volume integrals for active particle of the imaginary potentials. The next columns contain the theoretical cross sections calculated with various densities. On the left hand side of each of them are the r.m.s. radii of the corresponding imaginary potentials shown in Fig. 3. Typically an increase of 5% in the r.m.s. value results in a similar increase in the calculated reaction cross section, similarly to what we have noticed for the n-target potential. The values of Table 3 indicate that the volume integrals are the same for all densities as they are normalized to the number of particles while the r.m.s are different. However they obviously depend on the energy and on the method used to build the potential. On the other hand for each double folded potential the r.m.s. are independent of the energy because they are just determined by the densities. This is consistent with the results of Ref. [40]. The accuracy of our results can be discussed for example in comparison to Ref. [31, 32]. In that work the data for ^{12}C+^{12}C elastic scattering were studied at 100A MeV using microscopic coupled-channel calculations with the explicit

goal to check the effect of repulsive three-body forces. The potential between the colliding nuclei was determined by the double folding method with three different complex g-matrix interactions, and also the reaction cross section was calculated. The calculated value which agreed better with the data was σ_R = 950 mb, obtained with the MPa interaction [34] and a renormalization factor N_W = 0.57 for the imaginary potential. The MPa interaction includes repulsive three-body forces. It is interesting to note that with our single folded potential we obtain 969 mb and 953 mb with the HFB and HF densities respectively, without any renormalization for the potential, while the experimental value is 962 mb. With the double folded potential and the HFB densities we obtain 980 mb. Also similarly to what is shown in Fig. 4 and Table 3 for the double folded and single folded potentials at 300 MeV, we find that at 100 MeV the depth of the double folded potential should be renormalized by a factor 0.4 with respect to the single folded potential depths to make their values similar. However as noticed at 300 MeV, also at 100 MeV the r.m.s. radii would be very different, namely r.m.s.=3.75 fm and 3.43 fm for the single folded and double folded potentials respectively. This confirms the fact that a simple double folded potential calculated according to Eq. (4,5) would be far too absorptive because it does not contain *in-medium* effects which instead are partially contained in the microscopic potential of Ref. [32] thanks to the introduction of the three-body repulsive force. Thus such potentials need a not too strong renormalization. In light of such microscopic method results, one possible interpretation for our surface dominated n-T phenomenological potentials which give rise to relatively shallow but "wide" NN potentials, cf. Figs. 2 [LHS] and 3, is that they contain in a effective way the effects of short range repulsion pushing most nn interactions to the surface. Another interesting comparison can be done with the MOL method of Ref. [16], in particular their Eq. (10)

$$\exp\left(i\tilde{\chi}_{OLA}(\mathbf{b})\right) = \exp\left(-\int d\mathbf{b}\rho_p(\mathbf{b})\Gamma_{NT}(\mathbf{b}+\xi)\right)$$

could be interpreted as a single folded model in which the factor Γ_{NT} would be the result of the z-integration of an effective nucleon-target imaginary potential of gaussian shape

$$W_{MOL}(\mathbf{r}) = \frac{1}{2}\hbar v\left(\sigma_1\frac{e^{-r^2/2\beta_1}}{(2\pi\beta_1)^{3/2}} + \sigma_2\frac{e^{-r^2/2\beta_2}}{(2\pi\beta_1)^{3/2}}\right)$$

with $\sigma_{1,2}$ and $\beta_{1,2}$ given by the values in Table I of [16] and ρ_p given by Eq. (75) and Table 2 of [50]. Such a potential, shown in Fig. 2 [LHS] by the blue line for n+^{12}C shows a repulsive behaviour at very short distances which could be an effective representation of the short distance repulsion originating in the three-body terms of the chiral interaction as used for example in [32]. On the other hand in Fig. 3 the full magenta line with blue dots shows the corresponding NN imaginary potential for the system ^{12}C+^{12}C at 300A MeV. It has a volume integral of 184 MeVfm^3 and r.m.s=3.48 fm, consistent with our single folded results of Table 3. In particular we notice the same large distance behaviour as our best single folded potential. The modifications to the MOL introduced in Ref. [12] might represent an effective way to obtain the correct energy and radial dependence of their "effective" NT interaction.

From the discussion above it appears that Hartree-Fock and HFB densities are the best to reproduce the experimental reaction cross section values and indeed they are used in most codes related to exotic nuclei reactions. In Table 3 we compare results obtained with the NCSM and the HF and HFB densities. The energies of the scattering and cross sections and other relevant parameters are given. In particular as a significative parameter we provide also the *strong-absorption radius parameter* r_s extracted from $R_s = r_s(E_{inc})(A_P^{1/3} + A_T^{1/3})$ where R$_s$ [51, 52], is obtained from the S-matrices as the distance where $|\, S_{PT}(R_s)\,|^2 = \frac{1}{2}$. The values of this parameter in Table 3 indicate also that the single folded potentials provide longer range absorption than the double folded potential.

Fig. 4 presents the energy dependence of the calculated and experimental reaction cross sections [9, 12] for ^{12}C+^{12}C, and ^{9}Be+^{12}C. There are two curves showing results obtained within the single folded model: one (dot-dashed line), obtained using in the phenomenological imaginary part of the n-T potential the radius parameter r^I which depends on the incident energy according to Table 2, provides the best agreement with the data while the other (dashed line) obtained with the standard r^I=1.3 fm corresponds to values larger than the data. The full lines are double folded results which are in between the two single folded curves. What we have found is interesting because it agrees with what has been

discussed in other works like Ref. [12]. Namely it shows that modifications might be necessary in reaction models when including ingredients which successfully reproduce simpler reactions. In the case of the double folded model it is evident that not only the idea of a NN reaction being a collection of nn free reactions is too simple but it is also too simple the single folded description of a collection of free nucleons interacting with a nucleus via optical model potentials. However, at the moment it seems that simple, understandable modifications are sufficient to reproduce the data. For example, the reduction in the radius parameter found useful in our model might indicate that, when a nucleus scatters from another nucleus, as the energy increases its nucleons interact with those of the other nucleus at smaller distances than a free nucleon interacts with the nucleons of a nucleus.

4 Conclusions

In this talk we have discussed an excellent phenomenological n-^{12}C optical potential which fits the total cross sections up to 500 MeV. We have also single folded it with various projectile densities and have studied the systems ^{12}C+^{12}C, ^{9}Be+^{12}C finding that the energy dependence of the reaction cross section data can be fitted introducing a simple energy dependence in the radius parameter of the imaginary n-target potential. Single folded potentials have also been calculated and it has been shown once again that they are too deep and too "narrow". On the other hand we have shown that the MOL method to calculate phase shifts in which nucleon-target multiple scattering effects are taken into account provides potentials with characteristics similar to ours. The general conclusion of our study is then that it is necessary that the imaginary part of microscopic and/or semi-phenomenological optical potentials contains higher order and in medium effects. Also it would be useful to study further the importance of short range repulsion and the effect of the three-body force which might be at the origin of the necessary reduction of the strength of the potential at short distances. As a next step we intend to apply our single folded method to the evaluation of the S-matrices necessary in the eikonal formalism of nuclear breakup.

Acknowledgements

We are very grateful to Mack Atckinson for providing us with the unpublished calculations with the (DOM) potential shown in Fig. 1 [LHS] and to Petr Navrátil and Michael Gennari for the numerical values of the NCSM densities.

References

[1] F. Luoni, F. Horst, C A Reidel, A. Quarz, L .Bagnale, L. Sihver, U. Weber, R. B. Norman, W. de Wet, M. Giraudo, G. Santin, J. W. Norbury and M. Durante, New Journal of Physics **10**, 101201 (2021). https://dx.doi.org/10.1088/1367-2630/ac27e1

[2] T. D. Malouff, A. Mahajan, S. Krishnan, C. Beltran, D.S. Seneviratne and D. M. Trifiletti, Front. Oncol. 10:82. doi: 10.3389/fonc.2020.00082 https://kcch.kanagawa-pho.jp/i-rock/english/medical/

[3] S. Kunieda et al., Eur. Phys. J. A **59**, 2 (2023)

[4] D. Boscolo et al., Front. Oncol. **11**, 737050 (2021) https://doi.org/10.3389/fonc.2021.737050

[5] R. J. Glauber, in: W. E. Brittin, L. G. Dunham (Eds.), Lectures in Theoretical Physics, Vol. 1, Interscience, New York, 1959, p. 315

[6] G. R. Satchler and W. G. Love, Phys. Rep. **55**, 183 (1979)

[7] G.R. Satchler, Proceedings of La Rabida international Summer School on Heavy Ion Collisions, La Rabida (Huelva) Spain,June 7-19, 1982. https://inis.iaea.org/search/search.aspx?orig_q=RN:14722968

[8] R. M. De Vries, J. C. Peng, Phys. Rev. C **22**, 1055 (1980)

[9] S. Kox et al., Phys. Rev. C **35**, 1678 (1987)

[10] I. Tanihata et al., Phys. Lett. B **160**, 380 (1985)

[11] B. Abu-Ibrahim, W. Horiuchi, A. Kohama and Y. Suzuki, Phys. Rev. C **77**, 034607 (2008)
[12] M. Takechi, et al., Phys. Rev. C **79**, 061601(R) (2009)
[13] M. Tanaka et al., Phys. Rev. Lett. **124**, 102501 (2020)
[14] W. Horiuchi, Y. Suzuki, B. Abu-Ibrahim, and A. Kohama, Phys. Rev. C **75**, 044607 (2007)
[15] A. Ozawa et al., Nucl. Phys. A **691**, 599 (2001). A. Ozawa, AIP Conf. Proc. 865, 57 (2006); http://dx.doi.org/10.1063/1.2398828
[16] B. Abu-Ibrahim and Y. Suzuki, Phys. Rev. C **61**, 051601(R) (2000), Phys. Rev. C **62**, 034608 (2000)
[17] I. Tanihata, H. Savajols, R. Kanungo, Prog. Part. Nucl. Phys. **68**, 215 (2013), and references therein
[18] D. T. Tran, et al., Phys. Rev. C **94,** 064604 (2016)
[19] A. Bonaccorso, Prog. Part. Nucl. Phys., **101**, 1 (2018), and references therein
[20] C. Hebborn, T. R. Whitehead, A. E. Lovell, and F. M. Nunes, Phys. Rev. C **108**, 014601 (2023)
[21] M. S. Hussein, R. A. Rego, C. A. Bertulani, Phys. Rep. **201**, 279 (1991)
[22] C. A. Bertulani, and C. De Conti, Phys. Rev. C **81**, 064603 (2010)
[23] W. H. Dickhoff and R. J. Charity, Prog.Part. Nucl. Phys. **105**, 252 (2019)
[24] M. Burrows, C. Elster, S. P. Weppner, K.D. Launey, P. Maris, A. Nogga and G. Popa, Phys. Rev. C **99**, 044603 (2019)
[25] A. Idini, C. Barbieri, P. Navrátil, Phys. Rev. Lett. **123**, 092501 (2019)
[26] M. Vorabbi, M. Gennari, P. Finelli, C. Giusti, P. Navrátil, and R. Machleidt, Phys. Rev. C **103**, 024604 (2021)
[27] P. Finelli, M. Vorabbi, C. Giusti, J. Phys.: Conf. Ser. 2453, 012026 (2023), and references therein
[28] D. R. Entem, R. Machleidt, and Y. Nosyk, Phys. Rev. C **96**, 024004 (2017)
[29] T. Furumoto, K. Tsubakihara, S. Ebata, W. Horiuchi, Phys. Rev. C **99**, 034605 (2019)
[30] T. Furumoto, Y. Sakuragi, and Y. Yamamoto Phys. Rev. C **78**, 044610 (2008)
[31] T. Furumoto, W. Horiuchi, M. Takashina, Y. Yamamoto, and Y. Sakuragi Phys. Rev. C **85**, 044607 (2012)
[32] W. W. Qu et al., Phys Rev. C **95**, 044616 (2017) and references therein
[33] M. Toyokawa, M. Yahiro, T. Matsumoto, K. Minomo, K. Ogata, and M. Kohno, Phys. Rev. C **92**, 024618 (2015) and references therein
[34] Y. Yamamoto, T. Furumoto, N. Yasutake, and Th.A. Rijken, Eur. Phys. J. A **52**: 19 (2016)
[35] Y. P. Xu and D. Y. Pang, Phys. Rev. C **87**, 044605 (2013)
[36] J. P. Jeukenne, A. Lejeune, and C. Mahaux, Phys. Rev. C **16**, 80 (1977)
[37] E. Bauge, J. P. Delaroche, and M. Girod, Phys. Rev. C **63**, 024607 (2001)
[38] A. Bonaccorso and R. J. Charity, Phys. Rev. C **89**, 024619 (2014)
[39] A. Bonaccorso, F. Carstoiu, R. J. Charity, R. Kumar and G. Salvioni, Few-Body Syst. **57**, 331 (2016)
[40] A. Bonaccorso, F. Carstoiu, R. J. Charity, Phys. Rev. C **94**, 034604 (2016)
[41] I. Moumene and A. Bonaccorso, Nucl. Phys. A **1006** 122109 (2021)
[42] EXFOR nuclear data library [http://www.nds. iaea.org/exfor/exfor.htm]
[43] M. Atckinson, private communication
[44] Jin Lei, A. Bonaccorso, Phys. Lett. B **813**, 136032 (2021)
[45] R. B. Wiringa, R. Schiavilla, S. C. Pieper, J. Carlson, Phys. Rev. C **89**, 024305 (2014)
A. Piarulli, et al., Phys. Rev. C 107, 014314 (2023). https://www.phy.anl.gov/theory/research/density/ and references therein
[46] V. Somà, P. Navrátil, F. Raimondi, C. Barbieri, and T. Duguet, Phys. Rev. C **101**, 014318 (2020) and private communication
[47] M. V. Stoitsov et al., Comp. Phys. Comm. **184**, 1592, 2013, DOI: 10.1016/j.cpc.2013.01.013
M.V. Stoitsov, J. Dobaczewski, W. Nazarewicz, P. Ring, Comp. Phys. Comm. **167**, 43 (2005)
[48] J. Bartel, E. Quentin, M. Brack, C. Guet and H.-B. Hakansson, Nucl. Phys. A **386**, 79 (1982)
[49] P. Schwaller et al., Nuclei. Phys. A **316**, 317 (1979)

[50] Y. Ogawa, K. Yabana, and Y. Suzuki, Nucl. Phys. A **543**, 722 (1992)
[51] R. Bass, *Nuclear Reactions with Heavy Ions*, Springer-Verlag, Berlin, Heidelberg, New York, 1980, Sec. 3.3
[52] A. Bonaccorso, D. M. Brink and L. Lo Monaco, J. Phys. G **13**, 1407 (1987)